Article

A Direct Dynamics Trajectory Study of F + CHOOH Reactive Collisions Reveals a Major Non-IRC Reaction Path

Jos G. Lpez, Grigoriy Vayner, Upakarasamy Lourderaj, Srirangam V. Addepalli, Shuji Kato, Wibe A. deJong, Theresa L. Windus, and William L. Hase

J. Am. Chem. Soc., **2007**, 129 (32), 9976-9985• DOI: 10.1021/ja0717360 • Publication Date (Web): 21 July 2007

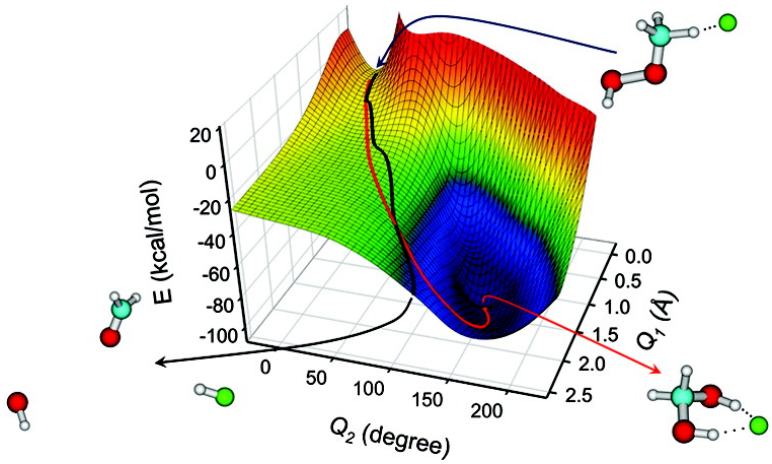

More About This Article

Additional resources and features associated with this article are available within the HTML version:

- Supporting Information
- Links to the 12 articles that cite this article, as of the time of this article download
- Access to high resolution figures
- Links to articles and content related to this article
- Copyright permission to reproduce figures and/or text from this article

View the Full Text HTML

J|A|C|S
ARTICLES
Published on Web 07/21/2007

A Direct Dynamics Trajectory Study of $F^- + CH_3OOH$ Reactive Collisions Reveals a Major Non-IRC Reaction Path

José G. López,[†] Grigoriy Vayner,[†] Upakarasamy Lourderaj,[†] Srirangam V. Addepalli,[†] Shuji Kato,[‡] Wibe A. deJong,[§] Theresa L. Windus,[§] and William L. Hase*,[†]

Contribution from the Department of Chemistry and Biochemistry, Texas Tech University, Lubbock, Texas 79409, Department of Chemistry and Biochemistry, University of Colorado, Boulder, Colorado 80309, and Environmental Molecular Science Lab, Pacific Northwest National Laboratory, Richland, Washington 99352

Received March 12, 2007; E-mail: bill.hase@ttu.edu

Abstract: A direct dynamics simulation at the B3LYP/6-311+G(d,p) level of theory was used to study the $F^- + CH_3OOH$ reaction dynamics. The simulations are in excellent agreement with a previous experimental study (*J. Am. Chem. Soc.* **2002**, *124*, 3196). Two product channels, $HF + CH_2O + OH^-$ and $HF + CH_3OO^-$, are observed. The former dominates and occurs via an $E_{CO}2$ mechanism in which F^- attacks the CH_3- group, abstracting a proton. Concertedly, a carbon−oxygen double bond is formed and OH^- is eliminated. Somewhat surprisingly this is not the reaction path, predicted by the intrinsic reaction coordinate (IRC), which leads to a deep potential energy minimum for the $CH_2(OH)_2\cdots F^-$ complex followed by dissociation to $HF + CH_2(OH)O^-$. None of the direct dynamics trajectories followed this path, which has an energy release of −63 kcal/mol and is considerably more exothermic than the $E_{CO}2$ path whose energy release is −27 kcal/mol. Other product channels not observed, and which have a lower energy than that for the $E_{CO}2$ path, are $F^- + CO + H_2 + H_2O$ (−43 kcal/mol), $F^- + CH_2O + H_2O$ (−51 kcal/mol), and $F^- + CH_2(OH)_2$ (−60 kcal/mol). Formation of the $CH_3OOH\cdots F^-$ complex, with randomization of its internal energy, is important, and this complex dissociates via the $E_{CO}2$ mechanism. Trajectories which form $HF + CH_3OO^-$ are nonstatistical events and, for the 4 ps direct dynamics simulation, are not mediated by the $CH_3OOH\cdots F^-$ complex. Dissociation of this complex to form $HF + CH_3OO^-$ may occur on longer time scales.

1. Introduction

An important concept in chemical kinetics is the reaction path, often defined by the intrinsic reaction coordinate (IRC).[1] This path connects stationary points on the potential energy surface (PES) and is determined by following steepest descent trajectories from saddle points to minima with the kinetic energy they acquire continuously removed.[2] The reaction path model may be combined with statistical theories[3] to make predictions concerning the kinetics of a chemical reaction.

A question of considerable interest is how accurately IRCs and statistical theories identify the actual atomic-level mechanisms for chemical reactions. This is particularly important for post-transition state dynamics where, after passing a rate controlling transition state, the PES may have a "rough" landscape, with multiple potential energy minima, reaction pathways, low-energy barriers, etc., connecting the transition state to multiple product channels. For low-pressure gas-phase conditions, where deactivating collisions are unimportant and the total energy is constant, the statistical model is RRKM theory,[4] which may be used to predict the time spent in each potential energy minima and the probabilities for transitions between minima and forming products. For a reaction in solution or involving a macromolecule with many degrees of freedom, the statistical model assumes that there is rapid energy transfer forming a Boltzmann distribution so that transition state theory may be used to calculate the unimolecular lifetimes of intermediates and probabilities of forming products.

Several chemical dynamics simulations have shown that for some reactions the post-transition state dynamics do not follow IRCs and, instead, the trajectories follow dynamical pathways. Such non-IRC dynamics was found for cyclopropyl radical ring opening,[5] the $OH^- + CH_3F \rightarrow CH_3OH + F^-$ S_N2 reaction,[6] in 1,2,6-heptatriene rearrangement,[7] and in the heterolysis rearrangement of protonated pinacolyl alcohol.[8] In recent work non-IRC dynamics has been identified for H_2CO and CH_3CHO

[†] Texas Tech University.
[‡] University of Colorado.
[§] Pacific Northwest National Laboratory.

(1) Fukui, K. *J. Phys. Chem.* **1970**, *74*, 4161.
(2) Ishida, K.; Morokuma, K.; Komornicki, A. *J. Chem. Phys.* **1977**, *66*, 2153.
(3) Moylan, C. R.; Brauman, J. I. In *Advances in Classical Trajectory Methods, Vol. 2, Dynamics of Ion-Molecule Complexes*; Hase, W. L., Ed.; JAI Press Inc.: Greenwich, CT, 1994; p 95.
(4) Baer, T.; Hase, W. L. *Unimolecular Reaction Dynamics: Theory and Experiments*; Oxford University Press: New York, 1996.
(5) Mann, D. J.; Hase, W. L. *J. Am. Chem. Soc.* **2002**, *124*, 3208.
(6) Sun, L.; Song, K.; Hase, W. L. *Science* **2002**, *296*, 875.
(7) Debbert, S. L.; Carpenter, B. K.; Hrovat, D. A.; Borden, W. T. *J. Am. Chem. Soc.* **2002**, *124*, 7896.
(8) Ammal, S. C.; Yamataka, H.; Aida, M.; Dupuis, M. *Science* **2003**, *299*, 1555.

10.1021/ja0717360 CCC: $37.00

Table 1. Geometries at Selected Stationary Points for the $F^- + CH_3OOH$ Reaction[a]

	geometry									
	$CH_3OOH\cdots F^-$					TS1				
theory	R_{F-H_4}	$R_{O_2-H_4}$	$R_{O_1-O_2}$	$\theta_{F-H_4-O_2}$	$\theta_{C-O_1-O_2}$	R_{F-H_1}	R_{H_1-C}	$R_{O_1-O_2}$	θ_{F-H_1-C}	$\theta_{C-O_1-O_2}$
MP2/6-311+G(d,p)	1.267	1.103	1.453	176.4	105.8	1.246	1.305	1.613	173.6	110.6
DFT/6-31+G(d)	–	–	–	–	–	1.272	1.303	1.686	170.2	110.8
DFT/6-31+G(d,p)	1.261	1.125	1.462	176.4	106.8	1.297	1.278	1.642	170.3	110.8
DFT/6-311+G(d,p)	1.275	1.112	1.458	176.3	107.0	1.345	1.247	1.630	170.3	110.4
	TS2					$CH_2(OH)_2\cdots F^-$				
	R_{F-H_1}	R_{H_1-C}	$R_{O_1-O_2}$	θ_{F-H_1-C}	$\theta_{C-O_1-O_2}$	R_{F-H_4}	$R_{O_2-H_4}$	R_{C-O_2}	θ_{F-H_4-C}	$\theta_{O_1-C-O_2}$
MP2/6-311+G(d,p)	1.776	1.114	1.453	166.9	109.0	1.595	1.001	1.403	154.1	112.5
DFT/6-31+G(d)	1.749	1.122	1.464	168.1	109.6	–	–	–	–	–
DFT/6-31+G(d,p)	1.729	1.124	1.465	168.7	109.6	1.595	1.010	1.407	154.3	112.7
DFT/6-311+G(d,p)	1.730	1.122	1.462	167.9	109.9	1.614	1.005	1.405	153.8	112.8
	$F^-\cdots CH_3OOH$					$HF + CH_2O + OH^-$				
	R_{F-H_1}	R_{H_1-C}	$R_{O_1-O_2}$	θ_{F-H_1-C}	$\theta_{C-O_1-O_2}$	R_{H-F}	R^b_{O-H}	R_{C-O}	R_{C-H}	θ_{H-C-H}
MP2/6-311+G(d,p)	1.709	1.125	1.471	168.3	107.5	0.917	0.965	1.213	1.105	116.1
DFT/6-31+G(d)	1.647	1.142	1.495	167.0	109.0	0.938	0.975	1.209	1.109	116.3
DFT/6-31+G(d,p)	1.605	1.150	1.501	167.5	109.2	0.928	0.970	1.210	1.108	116.2
DFT/6-311+G(d,p)	1.607	1.148	1.503	167.2	109.3	0.922	0.966	1.202	1.108	115.9
expt[c]	–	–	–	–	–	0.917	0.964	1.203	1.101	116.2

[a] Bond lengths are in angstroms (Å), and angles are in degrees (deg). [b] Bond length for OH^-. [c] The experimental geometries of HF, OH^-, and CH_2O are from refs 50, 51, and 52, respectively.

dissociation via the C−H bond rupture channel.[9−11] The dissociating H-atom crosses a ridge on the PES and "falls" into the highly exothermic elimination dissociation channel forming H_2 from H_2CO and CH_4 from CH_3CHO. Non-IRC dynamics for such a "roaming H-atom" mechanism was also observed in earlier studies of H-atom transfer.[12,13] It is also noteworthy that non-IRC dynamics has also been identified and explained for the $H + HBr \rightarrow H_2 + Br$ and $O(^3P) + CH_3 \rightarrow H_2 + H + CO$ reactions.[14,15] Non-IRC and non-TS dynamics are prevalent in high-energy collisions, where the reactive system traverses regions of the PES far above potential minima, IRCs, and TSs.[16,17]

In recent experiments, Kato and co-workers studied the 300 K kinetics of the base-mediated decomposition reaction $F^- + CH_3OOH$.[18] Much to their surprise, the reaction did not yield the most exothermic products $HF + CH_2(OH)O^-$ and the products predicted by the IRC. Instead, the much higher energy non-IRC products $HF + CH_2O + OH^-$ were formed. In the work presented here the results of a B3LYP/6-311+G(d,p) direct dynamics simulation are reported, which probe the post-transition state dynamics for the $F^- + CH_3OOH$ reaction. The results of the simulation agree with the previous experimental study and provide an atomic level understanding of the non-IRC dynamics.[6,17]

2. *Ab Initio* Energies and Potential Energy Surface

2.1. Stationary Point Properties. CBS-QB3, MP2, and B3LYP theories were used to calculate the geometries and frequencies of the reactants, transition states, intermediates, and products of the $F^- + CH_3OOH$ reaction. The structures and energies were calculated using the 6-311+G(d,p) basis set at the MP2 level of theory and the 6-31+G(d), 6-31+G(d,p) and 6-311+G(d,p) basis sets at the B3LYP level of theory. Vibrational frequencies were calculated at the MP2 and B3LYP levels of theory.

2.1.1. Geometries. The geometries at selected stationary points, optimized with the MP2 and B3LYP theories and different basis sets, are listed in Table 1 and depicted in Figure 1. Overall, the geometries calculated at the different levels of theory are in good agreement. The largest difference between the geometries, of the B3LYP/6-311+G(d,p) method used for the simulations and those for the MP2/6-311+G(d,p) method, is for the $F-H_1$ bond length of $F^-\cdots CH_3OOH$ and TS1. For the $F^-\cdots CH_3OOH$ complex the B3LYP value of the $F-H_1$ bond length is 0.1 Å shorter than that of MP2 theory. This difference is reversed for the TS1 transition state for which the B3LYP value is 0.1 Å larger.

2.1.2. Vibrational Frequencies. Vibrational frequencies were calculated for TS1, TS2, the $F^-\cdots CH_3OOH$ complex, and the $HF + CH_2O + OH^-$ products with the MP2 and B3LYP levels of theory and the 6-311+G(d,p) basis set and are listed in Table 2. These calculations were used to compare MP2 and B3LYP frequencies and to compare them with experiments. Overall the MP2 and B3LYP frequencies are in quite good agreement, with the largest difference for the O−O stretch of $F^-\cdots CH_3OOH$, i.e., 697 and 813 cm^{-1} for B3LYP and MP2, respectively. The frequencies of the $HF + CH_2O + OH^-$ products, given by the B3LYP/6-311+G(d,p) theory used for direct dynamics simulations, are in excellent agreement with experiment, with an average difference less than 2%. It is of interest that TS2 has higher frequencies than TS1. As discussed below, in section

(9) Townsend, D.; Lahankar, S. A.; Lee, S. K.; Chambreau, S. D.; Suits, A. G.; Zhang, X.; Rheinecker, J.; Harding, L. B.; Bowman, J. M. *Science* **2004**, 1158.
(10) Lahankar, S. A.; Chambreau, S. D.; Townsend, D.; Suits, F.; Farnum, J.; Zhang, X.; Bowman, J. M.; Suits, A. G. *J. Chem. Phys.* **2006**, *125*, 044303.
(11) Houston, P. L.; Kable, S. H. *Proc. Natl. Acad. Sci. U.S.A.* **2006**, *103*, 16079.
(12) ter Horst, M. A.; Schatz, G. C.; Harding, L. B. *J. Chem. Phys.* **1996**, *105*, 558.
(13) Troya, D.; González, M.; Wu, G.; Schatz, G. C. *J. Phys. Chem. A* **2001**, *105*, 2285.
(14) Pomerantz, A. E.; Camden, J. P.; Chiou, A. S.; Ausfelder, F.; Chawla, N.; Hase, W. L.; Zare, R. N. *J. Am. Chem. Soc.* **2005**, *127*, 16368.
(15) Marcy, T. P.; Díaz, R. R.; Heard, D.; Leone, S. R.; Harding, L. B.; Klippenstein, S. J. *J. Phys. Chem. A* **2001**, *105*, 8361.
(16) Meroueh, S. O.; Wang, Y.; Hase, W. L. *J. Phys. Chem. A* **2002**, *106*, 9983.
(17) Yan, T.; Doubleday, C.; Hase, W. L. *J. Phys. Chem. A* **2004**, *108*, 9863.
(18) Blanksby, S. J.; Ellison, G. B.; Bierbaum, B. V.; Kato, S. *J. Am. Chem. Soc.* **2002**, *124*, 3196.

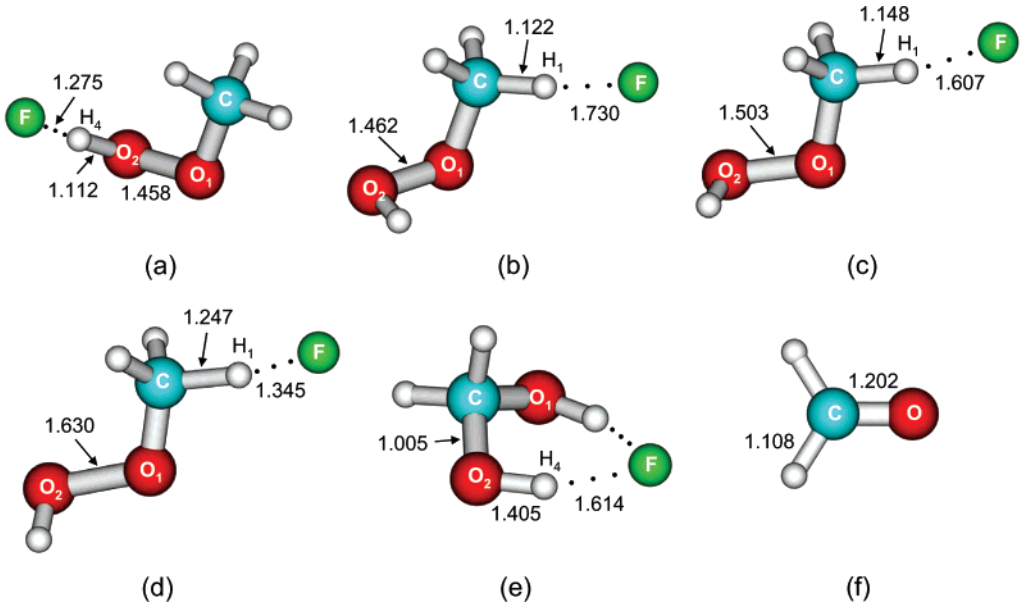

Figure 1. Geometries at selected stationary points, for the $F^- + CH_3OOH$ reaction, optimized with the B3LYP/6-311+G(d,p) level of theory. (a) $CH_3OOH\cdots F^-$, (b) TS2, (c) $F^-\cdots CH_3OOH$, (d) TS1, (e) $CH_2(OH)_2\cdots F^-$, and (f) CH_2O. Bond lengths in Å. The (···) identifies noncovalent interactions.

4.4, this has a significant effect on the unimolecular rate constants for $F^-\cdots CH_3OOH$ via TS1 and TS2 decomposition.

2.1.3. Energies. The CBS-QB3 energies were chosen as a benchmark for the accuracy of the calculations and were compared with energies calculated at the MP2 and B3LYP levels of theory. The resulting energies are listed in Table 3 and show that B3LYP theory gives a better accuracy than does MP2. According to experimental observations for this reaction,[18] the major reaction channel leads to the formation of $HF + CH_2O + OH^-$ via the transition state TS1. For this reaction pathway, B3LYP/6-311+G(d,p) gives a precision within 2 kcal/mol, while B3LYP/6-31+G(d,p), although good in most cases, results in a precision within 4 kcal/mol. Taking this into consideration, B3LYP/6-311+G(d,p) was chosen as most practical to perform the direct dynamics calculations of the $F^- + CH_3OOH$ reaction. The stationary point potential energies for the $F^- + CH_3OOH$ reaction pathways, at the chosen level of theory, are depicted in Figure 2. The difference in the B3LYP/6-311+G(d,p) and CBS-QB3 stationary point energies vary from 0.2 to 3.2 kcal/mol with the largest value of 3.2 kcal/mol for $HF + CH_3OO^-$, $CH_2(OH)_2\cdots F^-$, and $F^- + CO + H_2 + H_2O$.

2.2. Intrinsic Reaction Coordinate Calculation. The IRC connecting the transition state TS1 and the products was calculated at the B3LYP/6-311+G(d,p) level of theory. Energies and geometries along the IRC(*s*) are shown in Figure 3. The term *s* identifies the value of the reaction coodinate. The initial IRC involves H−F and O−H bond formation after rupture of the H−C and O−O bonds to form a tight $HF\cdots CH_2O\cdots HO^-$ complex. For *s* between 2 and 5 $amu^{1/2}$ Bohr, the IRC has a region with a less negative slope that involves OH^- motion away from CH_2O and rotation of this latter fragment. This rotation allows the migration of OH^- and HF toward the carbon and oxygen atoms of CH_2O, respectively, and a significant energy decrease. At an *s* of about 10 $amu^{1/2}$ Bohr, the IRC shows a complete relocation of the OH^- and HF fragments to form $HO\cdots C_2O^-\cdots HF$ followed by the formation of $HOCH_2O^-\cdots HF$ and, subsequently, $HOCH_2OH\cdots F^-$. At this point, the IRC enters an extremely shallow region in which the H···F end of the $HOCH_2OH\cdots F^-$ moiety slowly rotates toward OH to finally form the $CH_2(OH)_2\cdots F^-$ complex, which as illustrated in Figure 2 may dissociate to $HF + CH_2(OH)O^-$ or $CH_2(OH)_2 + F^-$.

3. Procedure for the Direct Dynamics Simulations

Ab initio direct dynamics trajectory calculations,[19−21] at the B3LYP/6-311+G(d,p) level of theory, were performed to investigate the dynamics of the $F^- + CH_3OOH$ reaction. Comparisons with other levels of theory, as described in section 2.1, show that the chosen level of theory is the most feasible for the simulations. The general chemical dynamics program VENUS,[22] interfaced with the electronic structure theory software package NWChem-4.7,[23] was used for the simulations.

3.1. Initial Conditions. The direct dynamics trajectories were initiated for the $F^- + CH_3OOH$ reactants, the TS1 transition state, and the $HOCH_2O^-\cdots HF$ IRC region of the potential energy surface and terminated after 4 ps or when the separation between the reaction products exceeded 16 Å. Quasiclassical sampling,[24] which includes zero-point energy, was used to select initial coordinates and momenta for the trajectories.

The $F^- + CH_3OOH$ trajectories were started at an initial 15 Å separation between F^- and the center of mass of CH_3OOH. The attractive potential is −0.21 kcal/mol at this separation for the most favorable $CH_3OOH\cdots F^-$ interaction. On the other hand, for this separation and the most favorable $F^-\cdots CH_3OOH$ interaction, the attractive potential is smaller and −0.13 kcal/mol. The reaction

(19) Bolton, K.; Hase, W. L.; Peslherbe, G. H. In *Modern Methods for Multidimensional Dynamics Computations in Chemistry*; Thompson D. L., Ed.; World Scientific: Singapore, 1998; p 143.
(20) Sun, L.; Hase, W. L. In *Reviews in Computational Chemistry, Vol. 19*; Lipkowitz, K., Larter, R., Cundari, T. R., Eds.; Wiley: New York, 2003; p 79.
(21) Hase, W. L.; Song, K.; Gordon, M. S. *Comput. Sci. Eng.* **2003**, *5*, 36.
(22) Hase, W. L.; Duchovic, R. J.; Hu, X.; Komornicki, A.; Lim, K. F.; Lu, D. H.; Peslherbe, G. H.; Swamy, S. R.; Vande Linde, S. R.; Varandas, A.; Wang, H.; Wolf, R. J. *Quantum Chemistry Program Exchange (QCPE) Bulletin* **1996**, *16*, 671.
(23) (a) Aprà, E., et al. *NWCHEM, a computational chemistry package for parallel computers*, version 4.7; Pacific Northwest Laboratory: Richland, WA 99352, 2005. (b) Kendall, R. A.; Aprà, E.; Bernholdt, D. E..; Bylaska, E. J.; Dupuis, M.; Fann, G. I.; Harrison, R. J.; Ju, J.; Nichols, J. A.; Nieplocha, J.; Straatsma, T. P.; Windus, T. L.; Wong, A. T. *Comput. Phys. Commun.* **2000**, *128*, 260.
(24) Peslherbe, G. H.; Wang, H.; Hase, W. L. In *Advances in Chemical Physics, Vol. 105, Monte Carlo Methods in Chemical Physics*; Ferguson, D. M., Siepman, J. I., Truhlar, D. G., Eds.; Wiley: New York, 1999; p 171.

Table 2. Harmonic Frequencies of Selected Stationary Points for the $F^- + CH_3OOH$ Reaction[a]

mode	MP2/6-311+G(d,p)	DFT/6-311+G(d,p)	expt[b]
	TS2		
F^- stretch	204i	193i	
F^- bend	85	90	
CH_3 torsion	163	183	
OOC wag	220	248	
OOH wag	298	315	
COO bend	508	490	
OO stretch	836	821	
CO stretch	1009	940	
CH_3 rock	1182, 1209	1152, 1189	
OOH rock	1335	1326	
CH_3 deformation	1489, 1520, 1567	1456, 1494, 1532	
CH_3 stretch	2799, 3082, 3154	2646, 3001, 3084	
OH stretch	3813	3752	
	$F^-\cdots CH_3OOH$		
F^- bend	89, 95	94, 104	
OOH wag	167	136	
F^- stretch	202	225	
CH_3 torsion	426	428	
COO bend	469	465	
OO stretch	813	697	
CO stretch	995	940	
CH_3 rock	1208, 1214	1179, 1189	
OOH rock	1310	1262	
CH_3 deformation	1513, 1526, 1533	1459, 1487, 1499	
CH_3 stretch	2654, 3058, 3109	2336, 2973, 3020	
OH stretch	3838	3778	
	TS1		
F^- stretch		461i	
OOH wag		96	
F^- bend		116, 131	
COO bend		325	
OO stretch		558	
CH_3 torsion		585	
CO stretch		1007	
OOH rock		1090	
CH_3 rock		1057, 1204	
CH_3 deformation		1310, 1414, 1490, 1523	
CH_3 stretch		2981, 2937	
OH stretch		3808	
	$HF + CH_2O + OH^-$		
HF stretch	4199	4097	4138
OH stretch	3838	3755	3738
CH_2 wag	1206	1198	1191
CH_2 rock	1278	1259	1299
CH_2 bend	1559	1531	1529
CO stretch	1762	1814	1778
CH_2 symmetric stretch	2976	2886	2978
CH_2 asymmetric stretch	3047	2944	2997

[a] Frequencies are in units of cm^{-1}. [b] The experimental harmonic frequencies of HF, OH^-, and CH_2O are from refs 50, 51, and 53, respectively.

dynamics following this latter attractive interaction is the principal focus of this work, and the small attractive potential indicates it is appropriate to use an initial separation of 15 Å. The initial separation would need to be increased substantially to significantly decrease the reactants' attractive interaction, and this would have a deleterious effect on the computational expense of the direct dynamics trajectories (see below).

Initial conditions for the CH_3OOH vibrational and rotational degrees of freedom were selected from their 300 K Boltzmann distributions. The initial relative translational energy E_{rel} equalled 0.89 kcal/mol, i.e., the average value of E_{rel} at the 300 K temperature of the $F^- + CH_3OOH$ experiments.[18] The collision impact parameter b was chosen randomly between zero and b_{max} (see discussion in the following section for the identification of b_{max}), and CH_3OOH had a random orientation with respect to F^-. The probability of a collision with a particular value of b is proportional to b, and the long-range interaction between F^- and CH_3OOH leads to collisions and chemical reactions with large b and, thus, large angular momentum.

A smaller ensemble of trajectories was also initiated at the TS1 transition state, which links the $F^- + CH_3OOH$ reactants with the products formed by F^- interacting with the CH_3- group of CH_3OOH. The trajectories were initiated at TS1 with a 300 K rotational angular momentum distribution. The angular momenta for this distribution are much lower than those which result from $F^- + CH_3OOH$ reactive collisions at large impact parameters, and it is of interest to see if the much lower 300 K rotational angular momentum affects the reaction dynamics. The initial conditions also included a 300 K energy distribution in reaction coordinate translation and a microcanonical ensemble of states for the vibrational modes orthogonal to the reaction coordinate. The energy for this ensemble corresponds to the reactant's 300 K thermal energy plus the potential energy difference between the reactants and TS1, i.e., 11.5 kcal/mol.

A small set of trajectories, initiated along the IRC, were also studied. Their initial IRC structure is $HOCH_2O^-\cdots HF$ and identified by the dot in Figure 3. Initial conditions for the modes orthogonal to the IRC were sampled for a microcanonical ensemble, with an energy equal to the reactant's thermal energy plus the potential energy difference between the reactants and $HOCH_2O^-\cdots HF$ structure. The reaction coordinate translation and external rotation energies were sampled from 300 K Boltzmann distributions.

3.2. Maximum Collision Impact Parameter for the $F^- + CH_3OOH$ Reaction. The collision impact parameter for each $F^- + CH_3OOH$ trajectory was randomly selected from zero to b_{max}. To assist in the evaluation of b_{max} the capture model[25] was used to estimate its value. This model is based on the effective potential

$$V_{eff}(R) = V(R) + \frac{\mu_R b^2 v_{rel}^2}{2R^2} \quad (1)$$

where R is the distance between F^- and the center of mass of CH_3OOH, $V(R)$ is the reactants' interaction potential, μ_R is the $F^- + CH_3OOH$ reduced mass, b is the collision impact parameter, and v_{rel} is the relative translational velocity. $V(R)$ was determined by assuming an equilibrium configuration for CH_3OOH and locating F^- along the $C-H_1$ bond line, as illustrated in Figure 4. Values of $V(R)$ were calculated at the B3LYP/6-311+G(d,p) level of theory used for the simulations, and v_{rel} was determined from the average relative translational energy at 300 K. Following the criterion for the capture model, b_{max} is the value of b for which the maximum of $V_{eff}(R)$ equals the initial relative translational energy E_{rel}. For $E_{rel} = 0.89$ kcal/mol used in the simulations, the resulting b_{max} is 11.3 Å. This b_{max} was used as a guide in choosing the actual value for the simulations. Sets of 10 $F^- + CH_3OOH$ trajectories were calculated at different values of b to determine the probability of F^- interacting attractively with CH_3OOH instead of directly scattering. For a b of 7.5 Å and less the probability of this attractive interaction is unity. However, for b in the range of 9.0−9.5 Å the combined probability for this attractive interaction is 0.06. For $b = 10$ Å each of the trajectories scattered directly, without an attractive interaction, and b_{max} was set to 10 Å for the $F^- + CH_3OOH$ simulations.

3.3. Trajectory Integration and Analysis. The trajectories were integrated using a Hessian-based predictor corrector algorithm[26] and implemented in the development version of VENUS/NWChem. The total energy was conserved to within 0.01 kcal/mol. The wall computer processing time for a single trajectory integrated for 4 ps required 5.7 days on a dedicated 3.2 GHz Xeon dual-processor with 4 GB RAM.

(25) Su, T.; Bowers, M. T. In *Gas Phase Ion Chemistry, Vol. 1*; Bowers, M. T., Ed.; Academic: New York, 1978; p 84.
(26) Lourderaj, U.; Song, K.; Windus, T. L.; Zhuang, Y.; Hase, W. L. *J. Chem. Phys.* **2007**, *126*, 044105.

Table 3. Electronic Structure Theory Energies for Stationary Points on the $F^- + CH_3OOH$ PES[a]

			MP2	DFT(B3LYP)		
structure	ZPE[b]	CBS-QB3	6-311+G(d,p)	6-31+G(d)	6-31+G(d,p)	6-311+G(d,p)
$HF + CH_3OO^-$	−2.5	1.7	5.8	7.6	5.9	4.9
$CH_3OOH\cdots F^-$	−0.3	−38.0	−36.0	−	−36.8	−36.5
TS2	−0.1	−12.2	−10.5	−11.7	−12.1	−12.4
$F^-\cdots CH_3OOH$	−0.6	−15.4	−13.8	−15.3	−15.9	−16.2
TS1	−3.1	−10.5	−9.7	−12.7	−14.6	−11.5
$CH_2(OH)_2\cdots F^-$	2.7	−108.0	−110.9	−	−103.3	−104.8
$HF + CH_2O + OH^-$	−6.8	−28.8	−35.2	−17.8	−22.8	−26.9
$F^- + CO + H_2 + H_2O$	−	−46.0	−55.6	−	−37.9	−42.8
$F^- + CH_2O + H_2O$	−4.0	−50.7	−57.6	−44.6	−47.7	−51.0
$F^- + CH_2(OH)_2$	1.3	−61.6	−66.1	−	−	−59.7
$HF + CH_2(OH)O^-$	−	−	−	−	−	−63.4

[a] Energies (kcal/mol) are with respect to $F^- + CH_3OOH$ and do not include zero-point energy (ZPE). [b] Zero-point energy with respect to that for $F^- + CH_3OOH$ and calculated at the B3LYP/6-311+G(d,p) level of theory. With this ZPE included the CBS-GB3 energy for $HF + CH_3OO^-$ is −0.8 kcal/mol.

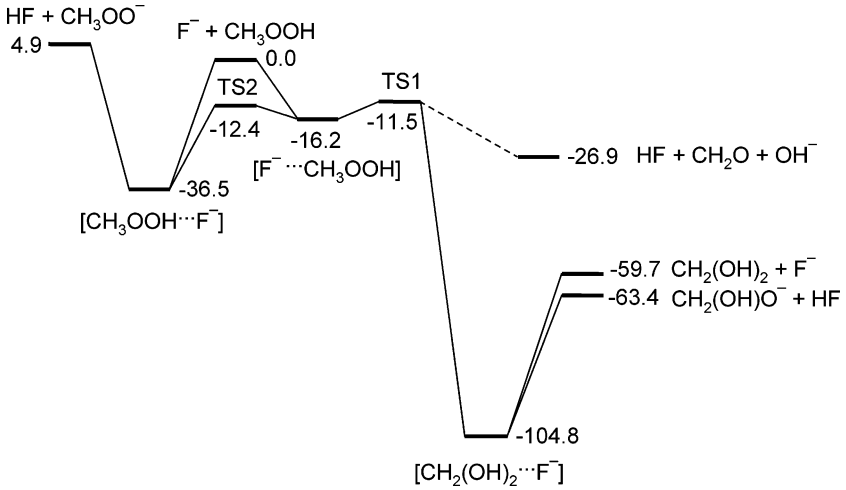

Figure 2. Energy diagram for the $F^- + CH_3OOH$ reaction at the B3LYP/6-311+G(d,p) level of theory. The energies shown are in kcal/mol and are relative to the $F^- + CH_3OOH$ reactant channel. Zero-point energies are not included.

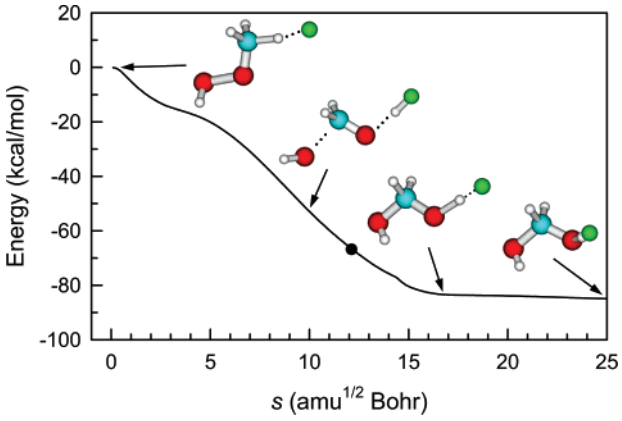

Figure 3. Potential energy along the IRC connecting the transition state TS1 and $CH_2(OH)_2\cdots F^-$ potential energy minimum. *s* is the distance along the IRC. The dot identifies the $HOCH_2O^-\cdots HF$ structure on the IRC, used to initiate some of the trajectories (see section 4.3). The potential energy at this point is −67 kcal/mol, with respect to the zero of energy for TS1.

The trajectories were analyzed for different types of events. The statistical uncertainty given, for the probability of a particular type of event, is 1 standard deviation (68% confidence level).[27]

(27) Truhlar, D. G.; Muckerman, J. T. In *Atom-Molecule Collision Theory: a Guide for the Experimentalist*; Bernstein R. B., Ed.; Plenum Press: New York, 1979; p 505.

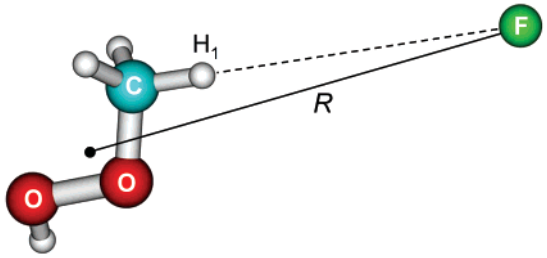

Figure 4. $F^- + CH_3OOH$ system for the calculation of b_{max} using the capture model. The dot indicates the position of the CH_3OOH center of mass, and the dashed line, the $C-H_1$ bond line along which F^- is located.

4. Results and Discussion

4.1. Dynamics of the $F^- + CH_3OOH$ Collisions. 200 trajectories were propagated in order to investigate the $F^- + CH_3OOH$ collision dynamics. Initial conditions were chosen for the trajectories as described above. The initial relative translational energy E_{rel} is 0.89 kcal/mol, the average relative translational energy for the 300 K temperature of the experiments.[18] Table 4 shows the number of trajectories for the different reaction channels found for the $F^- + CH_3OOH$ collisions. 23% formed $HF + CH_2O + OH^-$, the major product reaction channel observed in the experiment,[18] 48% became trapped in the $CH_3OOH\cdots F^-$ potential energy well and formed a reaction intermediate that lasted up to the 4 ps of the trajectory

Table 4. Total Number of Trajectories for the Different Product Channels[a]

	number of trajectories		
product	initiated at F^- + CH_3OOH[b]	initiated at TS1[c]	initiated at $HOCH_2O^-\cdots HF$[d]
$HF+CH_3OO^-$	3	0	0
$CH_3OOH\cdots F^-$	97	0	0
$HF+CH_2O+OH^-$	45[e]	76	5
$CH_2(OH)_2\cdots F^-$	0	0	0
F^- + CH_3OOH	55	0	0
minor products	0	4	0

[a] The trajectories are initiated in the reactant, TS1, and $HOCH_2O^-\cdots HF$ regions of the F^- + CH_3OOH potential energy surface. [b] 200 trajectories were initiated at the reactant channel. [c] 80 trajectories were initiated at TS1. [d] Five trajectories were initiated at the $HOCH_2O^-\cdots HF$ structure along the IRC. [e] Three of these events occurred by first forming the $CH_3OOH\cdots F^-$ complex.

integration, 1.5% formed the HF + CH_3OO^- reaction products, and the remaining trajectories went back to the reactants. None of the trajectories formed the IRC complex. The large fraction of trajectories trapped in the $CH_3OOH\cdots F^-$ potential energy well arises from the high-energy barriers between this complex and the HF + CH_3OO^- products and the $F^-\cdots CH_3OOH$ complex. The long lifetime for $CH_3OOH\cdots F^-$ is consistent with RRKM theory, as described in section 4.4. As discussed below in section 4.5, the fact that none of the trajectories followed the IRC is consistent with the experimental study.[18] The IRC complex and its dissociation products comprise, at most, only 2% of the total experimental product yield.

4.1.1. HF + CH_2O + OH^- Products. The vast majority of the trajectories that formed HF + CH_2O + OH^- followed the pathway depicted in Figure 5. The observation of this pathway provides theoretical evidence for the elimination mechanism proposed by Kato and co-workers[18] for base-mediated heterolytic decomposition of small alkyl hydroperoxides. Figure 5 clearly shows the association of the anion with an α-hydrogen (Figure 5b), crossing of the TS1 barrier (Figure 5c), and rupture of the C−H and O−O bonds (Figure 5d) to form formaldehyde, OH^-, and HF (Figure 5e). About 1.5 ps were required for the system to move from the reactants to the TS1 barrier, and an additional 0.7 ps was required to reach the 16 Å separation between the HF + CH_2O + OH^- reaction products. Only a small fraction of the trajectories (1.5%) entered the $CH_3OOH\cdots F^-$ potential well and then escaped through transition state TS2 to follow the pathway shown in Figure 5.

Comparison with the IRC, described above, shows that the trajectories that form HF + CH_2O + OH^- initially follow the IRC path up to s ~5 amu$^{1/2}$ Bohr. The dynamics of the trajectories show rupture of the H−C and O−O bonds after crossing the TS1 region, formation of a tight $HF\cdots CH_2O\cdots HO^-$ complex, and rotation of the CH_2O fragment. However, the dynamics leads to the separation of OH^- and HF from CH_2O instead of allowing formation of the $HO\cdots CH_2O^-\cdots HF$ IRC structure. The trajectories cease to follow the IRC when the slope of potential energy versus s becomes more negative at s ~5 amu$^{1/2}$ Bohr.

A two-dimensional contour diagram of the post-transition state potential energy surface, following motion from TS1, is illustrated in Figure 6. Q_1 represents the concerted movement of HF and OH^- away from CH_2O, and Q_2 represents the in-plane rotational motion of CH_2O. Also depicted in Figure 6 is the IRC and the motion for a representative trajectory. The

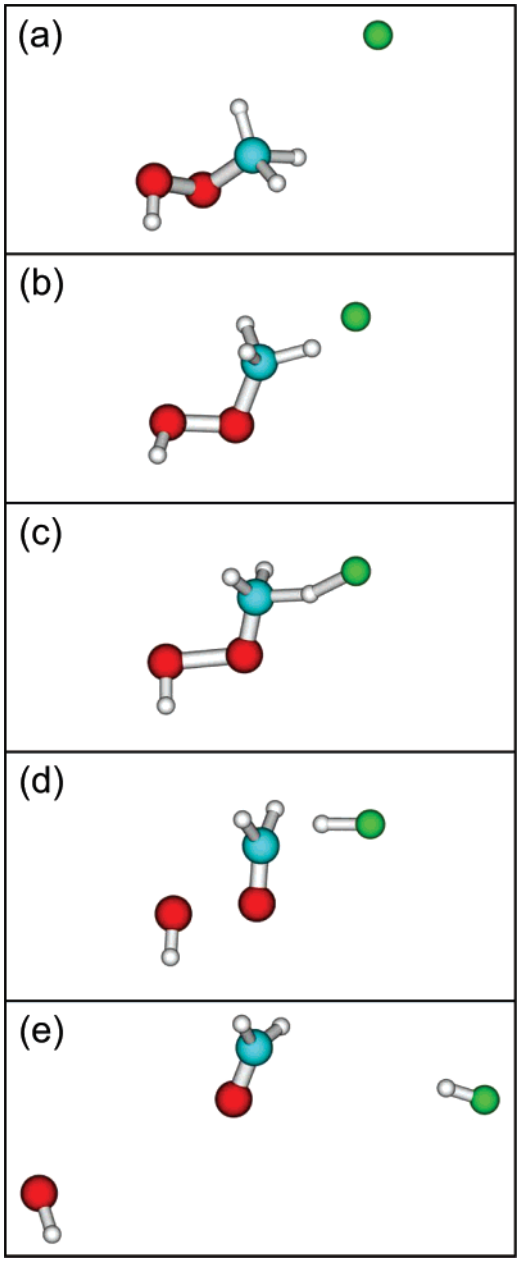

Figure 5. Representative trajectory showing the reaction pathway from the reactants to the major product channel HF + CH_2O + OH^- at (a) 990 fs, (b) 1086 fs, (c) 1108 fs, (d) 1116 fs, and (e) 1290 fs.

trajectory "skirts" the deep potential energy minimum of the $CH_2(OH)_2\cdots F^-$ IRC complex and has non-IRC dynamics reminiscent of those for the OH^- + $CH_3F \rightarrow CH_3OH$ + F^- reaction.[6]

4.1.2. HF + CH_3OO^- Products and $CH_3OOH\cdots F^-$ Complex. As shown in Table 4, three of the trajectories led to proton transfer from the hydroxyl group and the HF + CH_3OO^- products, while three of the $CH_3OOH\cdots F^-$ complexes, formed by the F^- + CH_3OOH collisions, dissociated to HF + CH_2O + OH^-. The PES suggests that the HF + CH_3OO^- product channel should proceed via the $CH_3OOH\cdots F^-$ complex, and since the barrier for this complex to dissociate to HF + CH_3OO^- is 16.4 kcal/mol (see Figure 2) higher than that to dissociate to HF + CH_2O + OH^-, it is somewhat surprising that there are the same number of events via this complex leading to HF + CH_3OO^- and to HF + CH_2O + OH^-. However, visualization

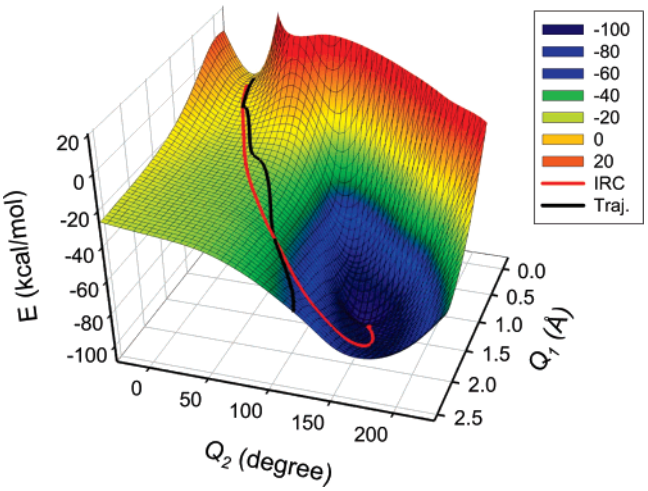

Figure 6. A two-dimensional contour diagram of the post-transition state potential energy surface for TS1. $Q_1 = \Delta r_1 + \Delta r_2$, where r_1 is the FH−C bond length and r_2 is the O−OH bond length. $Q_2 = \Delta\theta_1 + \Delta\theta_2$, where θ_1 is the O−C−O angle and θ_2 is the H−O−C angle; i.e., H is the hydrogen abstracted by F^-, and O is the oxygen attached to carbon. Q_1 represents the concerted motion of HF and OH^- away from CH_2O, and Q_2 represents rotation of CH_2O. The remaining coordinates were optimized for each Q_1, Q_2 point. Depicted on this contour diagram is the IRC (red line) and a representative trajectory (black line).

of the proton-transfer trajectories to form HF + CH_3OO^- shows that they are direct-type events and not mediated by a complex with randomization of its energy. For one of the trajectories HF is formed by a direct abstraction. For another the relative motion of F^- and the H-atom of H−O−O− reached its inner turning point (ITP) two times, which resulted from rotation as the proton is abstracted. For the third proton-transfer event the potential energy released, as F^- approaches the H−O−O− group, is localized in the F - - H - - O - moiety, resulting in multiple transfer of the H-atom between the F and O atoms. Proton transfer occurred after there were five ITPs in the F−H relative motion. In contrast, the three dissociations of the $CH_3OOH\cdots F^-$ complex to form the HF + CH_2O + OH^- products via the $E_{CO}2$ mechanism are more consistent with a statistical model. The lifetime of the complex varies from 0.45−2.1 ps for these three events, and as discussed below, the observation of three dissociations is consistent with RRKM theory.

There are several interesting aspects of the dynamics associated with formation of the $CH_3OOH\cdots F^-$ complex. For two of the trajectories, F^- approached the H-atom of the H−O−O− group but rebounded off to the CH_3− group forming HF + CH_2O + OH^-. For 19 of the trajectories, F^- bounced from the CH_3− to the H−O−O− group to form the $CH_3OOH\cdots F^-$ complex. These latter events are not surprising given the shallowness of the $F^-\cdots CH_3OOH$ potential energy minimum.

4.1.3. Nonreactive Trajectories. 55 of the trajectories were nonreactive and went back to the F^- + CH_3OOH reactants. For 42 of these trajectories F^- moved past CH_3OOH, scattering in the forward direction, but for the remaining 13 trajectories F^- scattered off CH_3OOH. The F^- ion hit the CH_3− group for 10 of these trajectories and rebounded with one inner turning point (ITP) in the F^- + CH_3OOH relative motion. One trajectory had similar dynamics, but F^- struck the OH− group. Two of the trajectories had a single ITP encounter with both the CH_3− and OH− groups. For one F^- first struck the CH_3− group, and for the other F^- first struck the OH− group. These trajectories, in which F^- scatters nonreactively off the CH_3− and OH− groups, would be identified as reactive events in a variational transition state theory analysis of the F^- + CH_3OOH chemical reaction.[28]

4.2. Trajectories Initiated at TS1. 80 trajectories were propagated starting at transition state TS1. Microcanonical sampling was used to determine the initial conditions for the trajectories with an energy corresponding to the thermal energy of the reactants plus the potential energy difference between the reactants and the TS1 structure. The reaction coordinate translational energy was sampled from its 300 K Boltzmann distribution. A 300 K rotational energy distribution was also added to TS1, which results in a much lower angular momentum than that created by the F^- + CH_3OOH reactive collisions. As seen in Table 4, 95% of the trajectories formed HF + CH_2O + OH^-. The remaining trajectories formed minor products such as HF + CO + H_2 + OH^-, F^- + CO + H_2 + H_2O, and HF + HCO^- + H_2O, which were not observed in the collision dynamics simulations discussed above (section 4.1). No evidence for formation of the IRC product was found for the trajectories initiated at TS1. The dynamics of the trajectories forming the primary products HF + CH_2O + OH^- is similar to that observed for the F^- + CH_3OOH collision dynamics (Figure 5c−e). As these trajectories moved from TS1 they followed the IRC, including the formation of a tight $HF\cdots CH_2O\cdots HO^-$ complex, followed by rotation of the CH_2O fragment and rearrangement of the HF and OH^- fragments, similar to that for the IRC path at an s of approximately 2−5 $amu^{1/2}$ Bohr. However, instead of continuing to follow the IRC to form $CH_2(OH)_2\cdots F^-$, the trajectories left the IRC and formed HF, OH^-, and CH_2O.

4.3. Trajectories Initiated at the $HOCH_2O^-\cdots$HF Structure on the IRC. Five trajectories were initiated at the $HOCH_2O^-\cdots$HF structure on the IRC, identified by the dot in Figure 3. Initial conditions were determined using a microcanonical sampling scheme. The energy for the trajectories was determined by adding the thermal energy of the reactants to the potential energy difference between the reactants and the $HOCH_2O^-\cdots$HF structure. In addition the energies for reaction coordinate translation and external rotation were sampled from their 300 K Boltzmann distributions. The motivation for this simulation was to see if initializing the trajectories far along the IRC, with a potential energy of −67 kcal/mol with respect to TS1, would direct them to the IRC products. However, each of the trajectories formed the HF + CH_2O + OH^- products with no evidence of following the IRC path.

4.4. RRKM Calculation. Quantum and classical RRKM calculations were performed for dissociation of the $CH_3OOH\cdots F^-$ complex via TS2 and TS1 using the B3LYP/6-311+G(d,p) frequencies and energies, the same level of theory used for the direct dynamics simulations. External rotations were treated with the adiabatic symmetric top approximation in calculating the sum and densities of states.[29] The total angular momentum was set to the average total angular momentum for the trajectories forming the $CH_3OOH\cdots F^-$ complex. Dissociation of $CH_3OOH\cdots F^-$ to the HF + CH_2O + OH^- products proceeds through TS2 and TS1, and the statistical rate constant for this process is

(28) Truhlar, D. G.; Hase, W. L.; Hynes, J. T. *J. Phys. Chem.* **1983**, *87*, 2664.
(29) Zhu, L.; Hase, W. L. *Chem. Phys. Lett.* **1990**, *175*, 117.

$$k = \frac{k_2 k_1}{k_1 + k_{-2}} \quad (2)$$

where the rate constants are for the reactions

$$CH_3OOH\cdots F^- \underset{k_{-2}}{\overset{k_2}{\rightleftharpoons}} F^-\cdots CH_3OOH$$

$$F^-\cdots CH_3OOH \xrightarrow{k_1} \text{products past TS1}$$

It is of interest that the quantum harmonic RRKM value for k_1 is ~10 times larger than the value for k_{-2}, since the barrier for k_1 is larger than that for k_{-2}. This is because TS2 has a much "tighter" structure, with higher vibrational frequencies, than does TS1.

The quantum harmonic RRKM value for k is 0.0018 ps^{-1}, and the RRKM lifetime $\tau = 1/k = 556$ ps. For the 4 ps trajectories, the dynamics of the $CH_3OOH\cdots F^-$ complex is followed on average for 2.3 ps. The RRKM value for the fraction of complexes which dissociate is $1 - \exp(-kt)$ with $t = 2.3$ ps. Thus, the RRKM percentage of trajectories which should dissociate is 0.4% and smaller than the 3% value found in our simulations; i.e., of the 100 complexes formed, 3 dissociated via TS2 and TS1 to form $HF + CH_2O + OH^-$.

Quantum RRKM theory retains a fixed amount of energy in zero-point energy (ZPE) for both the reactants and TS. However, classical dynamics does not necessarily preserve ZPE,[30,31] and if the classical intramolecular dynamics is ergodic the ZPE flows freely between the vibrational degrees of freedom of the decomposing molecule and TS. Thus, the barrier for decomposition is the classical potential energy barrier. The classical harmonic RRKM rate constant is larger than the quantum value,[32] and for $CH_3OOH\cdots F^-$ decomposition the classical harmonic RRKM rate constant k is 0.0155 ps^{-1} and 8.6 times larger than the quantum value. The percentage of the complexes predicted to decompose is 3.5% and in remarkably good agreement with the trajectory result of 3%. However, better trajectory statistics are needed to make this comparison more definitive. It is also possible there is an apparent non-RRKM[33] component in the dissociation of $CH_3OOH\cdots F^-$.

An important approximation in the RRKM calculations is the assumption of harmonic energy levels for both $CH_3OOH\cdots F^-$ and the transition states. Because the vibrational energy of $CH_3OOH\cdots F^-$ is higher than that of the transition states, the anharmonic correction is expected to be more important for the $CH_3OOH\cdots F^-$ density of states than the transition states sums of states. As a result, anharmonicity will decrease the rate constant by increasing the density of states. An anharmonic correction may be particularly important for the intermolecular degrees of freedom of $CH_3OOH\cdots F^-$, which represent the interaction of F^- with CH_3OOH.[34] Anharmonic effects are often important,[4] and it is noteworthy, that for a recent direct dynamics simulation of molozonide dissociation, an anharmonic correction of 2.2−2.6 was suggested.[35]

4.5. Comparison with Experiment. The dynamics of the $F^- + CH_3OOH$ reaction has been studied in previous experiments at 300 K utilizing a tandem flowing afterglow-selected ion flow tube (FA-SIFT) mass spectrometer.[18] The measured rate constant is $k = 1.23 \times 10^{-9}$ cm^3/molecule·s, and the major primary product is OH^-. A minor complication in determining the relative importance of the product channels is that OH^- undergoes a secondary reaction with CH_3OOH to form $H_2O + CH_3OO^-$. This latter ion is also formed by $F^- + CH_3OOH$ direct proton transfer. The importance of the $OH^- + CH_3OOH$ secondary reaction was unraveled by studying it separately. A numerical analysis of the experimental data, for $F^- + CH_3OOH$ and $OH^- + CH_3OOH$, suggests that the reaction of F^- with CH_3OOH proceeds mainly via the formation of OH^- (~85%) with an upper bound for direct proton transfer to form CH_3OO^- estimated to be approximately 10%.[18]

An $E_{CO}2$ mechanism was proposed for OH^- formation from the experimental results.[18] In this mechanism deprotonation from the α-carbon, by the attacking anion, leads to carbon−oxygen double bond formation with concerted elimination of the anionic leaving group. For the $F^- + CH_3OOH$ reaction, the products of the $E_{CO}2$ mechanism are $HF + CH_2O + OH^-$. Supporting evidence for the $E_{CO}2$ mechanism comes from studying the kinetics of the reverse reaction, $CH_3OO^- + HF$. Measurements with the FA-SIFT technique gives a rate constant of $k = 2.43 \times 10^{-9}$ cm^3/molecule·s and identifies, with 81% yield, OH^- as the primary reaction product. The proposal, based in part on *ab initio* calculations, is that the reactants form the $F^-\cdots CH_3OOH$ complex which then dissociates via the $E_{CO}2$ mechanism to form $HF + CH_2O + OH^-$.

The $F^- + CH_3OOH$ direct dynamics simulations reported here are in excellent agreement with the experimental measurements and the mechanistic details suggested from the experiments. The simulations identify the same $E_{CO}2$ mechanism for OH^- formation (see Figure 5) as proposed from the experiments. The direct dynamics rate constant is given by the expression $k = \langle v_{rel} \rangle \sigma_{rxn}$, where $\langle v_{rel} \rangle$ is the relative velocity for the average translational energy $3RT/2 = 0.89$ kcal/mol at 300 K and σ_{rxn} is the reaction cross section, and is given by $P_{rxn}\pi b_{max}^2$, where P_{rxn} is the reaction probability and the fraction of trajectories that react. From Table 4 $P_{rxn} = 145/200 = 0.73 \pm 0.03$. For $b_{max} = 10$ Å used in the simulations (see section 3.2), the resulting σ_{rxn} is 229 ± 10 $Å^2$, so that $k = (1.70 \pm 0.07) \times 10^{-9}$ cm^3/molecule·s and in quite good agreement with the experimental value 1.23×10^{-9} cm^3/molecule·s.

A direct comparison cannot be made with the ~85% and ~10% branching found from the experiments for the $HF + CH_2O + OH^-$ and $HF + CH_3OO^-$ product channels, since a large number of $CH_3OOH\cdots F^-$ complexes remain undissociated when the trajectories are terminated at 4 ps (see Table 4). However, if these complexes are assumed to dissociate statistically as predicted by RRKM, nearly all will form the $HF + CH_2O + OH^-$ products since the barrier is 16.4 kcal/mol lower for this channel. With this assumption, the branching between the $HF + CH_2O + OH^-$ and $HF + CH_3OO^-$ product channels is predicted to be $142/145 = 0.98 \pm 0.01$ and $3/145 = 0.02 \pm 0.01$, fractions in qualitative agreement with the experimental results. The experimental estimates of approximately 85% and 10% for these two channels are based on a difficult numerical analysis that subtracted a large contribution from the secondary

(30) Lu, D.; Hase, W. L. *J. Chem. Phys.* **1988**, *89*, 6723.
(31) Miller, W. H.; Hase, W. L.; Darling, C. L. *J. Chem. Phys.* **2006**, *91*, 2863.
(32) Hase, W. L.; Buckowski, D. G. *J. Comput. Chem.* **1982**, *3*, 335.
(33) Bunker, D. L.; Hase, W. L. *J. Chem. Phys.* **1973**, *59*, 4621.
(34) Peslherbe, G. H.; Wang, H.; Hase, W. L. *J. Chem. Phys.* **1995**, *102*, 5626.
(35) Vayner, G.; Addepalli, S. V.; Song, K.; Hase, W. L. *J. Chem. Phys.* **2006**, *125*, 14317.

reaction $OH^- + CH_3OOH \rightarrow CH_3OO^- + H_2O$.[36] Thus, the trajectory estimate of only ~2% branching to the HF + CH_3OO^- products is not inconsistent with the experiments.

The finding from the simulation, that none of the trajectories followed the IRC to form the $CH_2(OH)_2\cdots F^-$ complex, is also consistent with the experimental study.[18] If formed, the complex will contain ~110 kcal/mol of internal energy and is expected to undergo substantial dissociation to both HF + $CH_2(OH)O^-$ and F^- + $CH_2(OH)_2$, since the channels have barriers of only ~40−45 kcal/mol. The former dissociation channel was searched for in the experiments by studying the F^- + CD_3OOH reaction, for which formation and dissociation of the IRC complex would give DF + $CD_2(OH)O^-$. The proton transfer anion CD_3OO^- was observed, but the IRC product ion $CD_2(OH)O^-$ was not, indicating there was at most only a very small number of events which followed the IRC. A minor product with a 2% yield and corresponding to the mass of F^- + CH_3OOH was detected. Presumably this percentage corresponds to undissociated $CH_3OOH\cdots F^-$ complexes. It also sets an upper bound on the amount of the IRC complex produced. The most likely scenario is that the formation of the IRC complex is negligibly small (<2%).

5. Summary and Conclusions

The direct dynamics simulation reported here is in overall quite good agreement with previous experiments[18] and provides important fundamental information concerning the atomic-level reaction dynamics. As found from the experiments the primary product channel leads to HF + CH_2O + OH^- with the HF + CH_3OO^- proton abstraction channel considerably less important. The total rate constant for the F^- + CH_3OOH reaction, determined from the simulation, is $k = (1.70 \pm 0.07) \times 10^{-9}$ cm^3/molecule·s and in excellent agreement with the experimental value $k = 1.23 \times 10^{-9}$ cm^3/molecule·s.

Several features of the F^- + CH_3OOH reaction dynamics do not conform to conventional theories of chemical kinetics and dynamics. The reaction channel forming HF + CH_2O + OH^- occurs by an attractive interaction between F^- and the CH_3- group of CH_3OOH, while for HF + CH_3OO^- formation the F^- anion interacts with the H-atom of the H−O−O− group. The intrinsic reaction coordinate (IRC) reaction path model for the first channel, as described in Figure 3, is first formation of the $F^-\cdots CH_3OOH$ complex and then passage over TS1, followed by motion down the IRC to the $CH_2(OH)_2\cdots F^-$ potential energy minimum. The direct dynamics trajectories follow the initial features of this IRC reaction path model but then move off the IRC after passing TS1 and form the high-energy HF + CH_2O + OH^- products instead of going to the $CH_2(OH)_2\cdots F^-$ potential energy minimum or forming the F^- + CO + H_2 + H_2O and F^- + CH_2O + H_2O products at intermediate energies. Similar non-IRC reaction dynamics has been found in previous studies[5,6,8−14] for reactants at thermal energies.

As illustrated in Figure 3, collision of F^- with the H-atom of the H−O−O− group leads to the deep potential energy minimum for the $CH_3OOH\cdots F^-$ complex, which may decompose to HF + CH_3OO^- or HF + CH_2O + OH^- via TS2 and TS1. For the 4 ps trajectories reported here, these two product channels have equal probabilities. The atomic level dynamics of the simulations show that, in the early stages of the chemical reaction, the formation of the HF + CH_3OO^- products is nonstatistical and results from direct or nearly direct F^- + $CH_3OOH \rightarrow$ HF + CH_3OO^- proton-transfer events which are not mediated by randomization of vibrational energy within the $CH_3OOH\cdots F^-$ complex. These dynamics are similar to the direct reactions proceeding through potential energy minima for Cl^- + CH_3Cl and Cl^- + CH_3Br S_N2 nucleophilic substitution.[37−40] Nonstatistical dynamics for a heavy−light−heavy reactive system,[41] like F^- + H−O−O−, has also been observed for the $O(^1D)$ + HCl reaction.[42]

It would be very beneficial to have a semiquantitative or qualitative model for identifying reactions which may have non-IRC dynamics. Elements of such a model have been proposed previously[33,43,44] and observed in previous simulations as well as the one presented here. For some potential energy surfaces, there are multiple reaction paths crossing at a potential energy minimum, and in contrast to the RRKM model which assumes energy randomization and statistical branching between product channels, it has been proposed that there may be a propensity for the system to remain on the IRC and not become trapped in the potential energy minimum.[43] This type of dynamics has been observed in cyclopropane stereomutation[45−47] and S_N2 nucleophilic substitution.[39,48] The previous study of the OH^- + CH_3F post-transition state dynamics and the current F^- + CH_3OOH study suggest that the concept of momentum conservation and concomitant inefficient intramolecular vibrational energy redistribution (IVR)[33] should include motion off the IRC, resulting in non-IRC reaction paths. The presence of chemical dynamics with momentum conservation and weak mode coupling along either the IRC or a non-IRC reaction path is closely related to non-ergodic phase space dynamics and non-RRKM kinetics,[33] as seen for the dissociation of ion−dipole complexes[34,49] and central barrier recrossing[44] in S_N2 nucleophilic substitution reactions.[39] Developing a theoretical model to describe the above post-transition state non-IRC and nonstatistical dynamics would be an important contribution to the understanding of chemical kinetics and dynamics.

Acknowledgment. This material is based upon work supported by the National Science Foundation under Grant Nos. CHE-0412667 and CHE-0615321 and the Robert A. Welch

(36) A discussion of the uncertainty in the experimental estimate of the HF + CH_3OO^- product yield is given in footnote 9 of ref 18.

(37) Vande Linde, S. R.; Hase, W. L. *J. Am. Chem. Soc.* **1989**, *111*, 2349.
(38) Vande Linde, S. R.; Hase, W. L. *J. Chem. Phys.* **1990**, *93*, 7962.
(39) Hase, W. L. *Science* **1994**, *266*, 998.
(40) Wang, Y.; Hase, W. L.; Wang, H. *J. Chem. Phys.* **2003**, *118*, 2688.
(41) Fitz, D. E.; Brumer, P. *J. Chem. Phys.* **1979**, *70*, 5527.
(42) Martínez, T.; Hernández, M. L.; Alvariño, J. M.; Aoiz, F. J.; Sáez Rábanos, V. *J. Chem. Phys.* **2003**, *119*, 7871.
(43) Carpenter, B. K. *J. Am. Chem. Soc.* **1985**, *107*, 5730.
(44) Cho, Y. J.; Vande Linde, S. R.; Zhu, L.; Hase, W. L. *J. Chem. Phys.* **1992**, *96*, 8275.
(45) Doubleday, C., Jr.; Bolton, K.; Hase, W. L. *J. Am. Chem. Soc.* **1997**, *119*, 5251.
(46) Hrovat, D. A.; Fang, S.; Borden, W. T.; Carpenter, B. K. *J. Am. Chem. Soc.* **1997**, *119*, 5253.
(47) Doubleday, C., Jr.; Bolton, K.; Hase, W. L. *J. Phys. Chem. A* **1998**, *102*, 3648.
(48) Vande Linde, S. R.; Hase, W. L. *J. Am. Chem. Soc.* **1989**, *111*, 2349.
(49) Vande Linde, S. R.; Hase, W. L. *J. Phys. Chem.* **1990**, *94*, 6148.
(50) Huber, K.; Herzberg, G. *Molecular Spectra and Molecular Structure. IV. Constants of Diatomic Molecules;* Van Nostrand Reinhold Co.: New York, 1979.
(51) Rosenbaum, N. H.; Owrutsky, J. C.; Tack, L. M.; Saykally, R. J. *J. Chem. Phys.* **1986**, *84*, 5308.
(52) Duncan, J. L. *Mol. Phys.* **1974**, *28*, 1177.
(53) Reisner, D. E.; Field, R. W.; Kinsey, J. L.; Dai, H. L. *J. Chem. Phys.* **1984**, *80*, 5968.

Foundation under Grant No. D-0005. Support was also provided by the High-Performance Computing Center (HPCC) at Texas Tech University, under the direction of Philip W. Smith. Professor Kihyung Song is thanked for his assistance in the IRC calculation. S.K. acknowledges support from the National Science Foundation Grant No. CHE-0349937.

Supporting Information Available: Optimized geometries and electronic energies for Figure 1. This material is available free of charge via the Internet at http://pubs.acs.org.

JA0717360